Preprints of the 21st IFAC World Congress (Virtual)
Berlin, Germany, July 12-17, 2020

New modeling results for an EEG measurement system with exciting and reading electrodes

Mariana Mulinari Pinheiro Machado * **Alina Voda** *
Gildas Besançon * **Guillaume Becq** * **Olivier David** **

* *Univ. Grenoble Alpes, CNRS, Grenoble INP, GIPSA-lab, 38000 Grenoble, France (e-mail:{Mariana.Mulinari-Pinheiro-Machado,alina.voda,gildas.besancon,guillaume.becq}@grenoble-inp.fr)*
** *Univ. Grenoble Alpes, Grenoble Institut des Neurosciences, GIN, 38000 Grenoble, France (e-mail:olivier.david@univ-grenoble-alpes.fr)*

Abstract: In a context where electroencephalography (EEG) is largely used for brain studies, this paper focuses on the dynamics of the measurement process itself by means of a so-called *phantom EEG* device developed in a former study. A model is proposed in order to better understand the physical properties of each part of the measurement chain separately, with the purpose of helping for a better recovery of neuronal activity. The model structure is based on a physical analysis, and parametric identification is used in combination with it to estimate all the underlying physical components. Numerical results are provided based on experimental data.

Keywords: Electroencephalography (EEG) measurement chain, *phantom EEG*, electrode/electrolyte interface, non integer order model, modeling, identification.

1. INTRODUCTION

Electroencephalography (EEG) is largely used in neuroscience and medical diagnosis. It consists of the recording of electric potentials differences induced by current flows during neuronal activities. It is often realized on subject scalps with metal electrodes. Measurements acquired from EEG recordings can be useful in monitoring alertness and locating injured areas in the brain for example. In this report, we model the measurement chain of an EEG recording itself. To do so, a specific device was built (Becq et al. (2017)) called *phantom EEG* that mimics the measurement chain of such processes. This device gave rise to first transfer function models (Besançon et al. (2018)) and (Besançon et al. (2019)).

The purpose here is to refine these models by adding physical components described in the literature concerning EEG measurements, at different parts of the system. This enable to identify them precisely and can be helpful for modeling data in real EEG applications where the input sources are not controlled or where electrodes may interact differently with the medium depending on their locations in the brain. Furthermore, this enables to better relates these components to reactions occurring during the measurement process.

This paper is organized as follows: First, in section 2, the device considered is presented as well as an overview of the different parts of the measurement chain. In section 3 the new model is introduced, together with the parametric identification approach. In section 4 the results obtained with experimental data are shown and finally section 5 concludes this paper.

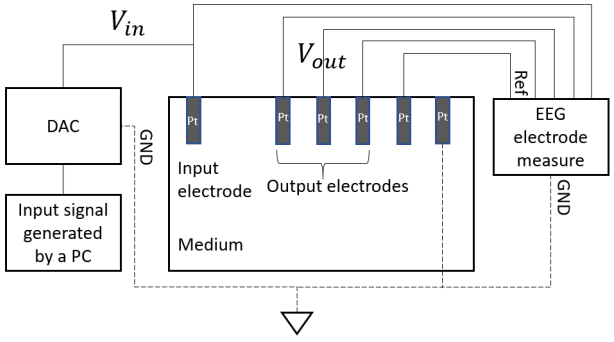

Fig. 1. Experimental setup for data acquisition of the *phantom EEG*.

2. EEG MEASUREMENT SYSTEM AND MODELING PROBLEM

The experimental setup proposed in Becq et al. (2017) can be represented as Fig. 1.

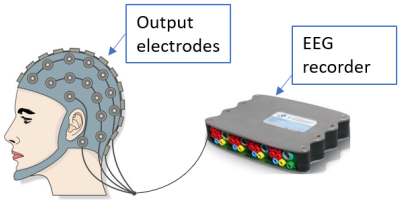

Fig. 2. Measurement chain components of an actual EEG recording

Copyright lies with the authors

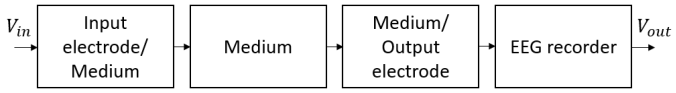

Fig. 3. Block diagram of the different parts of the EEG measurement chain.

The input signal is a white noise generated in Python that is transmitted to the input electrode via a digital to analog converter (National Instruments CRIO-9263 mounted on a cDAQ-9181 Ethernet chassis). The input electrode is inserted into an electrolyte medium which is a solution of phosphate buffered saline (PBS) obtained from a dissolution of half a tablet of P4417 Sigma-Aldrich dissolved in 1 l of pure water (0.1 times concentration). The output voltage is measured in three different positions by output electrodes located at 1 cm, 3 cm, and 5 cm from the input electrode. The input and output electrodes are connected to an EEG recorder (g.tec g.USBamp) with a selected sampling frequency of 4.8 kHz. The electrodes are made out of pure platinum and have a cylindrical shape with a 0.5 mm diameter and length of 1 cm. Only about 0.5 cm of the length of the electrodes are inserted into the medium. The translation of the components of the measurement chain to an actual EEG recording is shown in Fig. 2. In this case instead of an input signal generated by a PC, the signal measured by the output electrodes is the neuronal activity.

As it was mentioned before, the aim of the study is to understand the dynamics and physical properties of each stage in the EEG measurement chain. In other words, we would like to go beyond the direct transfer function between input voltage V_{in} and output voltage V_{out}, as it was established in Besançon et al. (2019), and find a model that describes separately the effects of input electrode, medium, output electrode and EEG recorder, as in Fig. 3.

3. IDENTIFICATION APPROACH AND PHYSICAL PARAMETERS RECOVERY

Differently from Besançon et al. (2019) where the transfer function to be identified was proposed by the analysis of the data in frequency, the transfer function in this article will be obtained from an electronic circuit whose components represent physical properties of each part of the measurement chain.

3.1 Physical-based approach for model structure

One of the first authors to propose an electronic circuit representation of the EEG measurement chain was Robinson (1968), with a form recalled in Fig. 4. The difference between the model proposed by Robinson and the *phantom EEG* being analysed in this paper is the input electrode. The signal is considered to be generated directly from neuronal activities. Robinson represents the solution by a resistance (R_s), the impedance of the output electrode by a metallic resistance (R_m) in series with the parallel of the shunt capacitance of the system to the ground (C_s) and the input impedance of the amplifier of the recorder (Z_a). Robinson also proposes a representation of the interface between the electrode and the electrolyte solution as the parallel between a double layer capacitance C_{dl} and a charge transfer resistance R_{CT}.

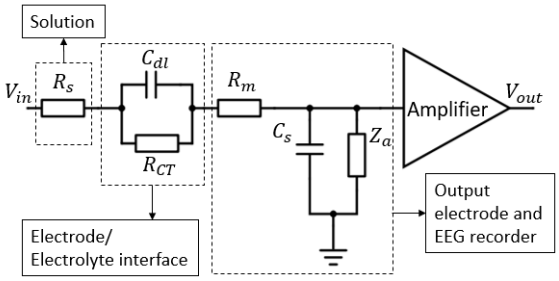

Fig. 4. Model proposed in Robinson (1968) for EEG measurement chain with input from neuronal activity.

Many authors have discussed fractional order representations of the electrode/electrolyte interface. For instance Magin and Ovadia (2008) studied the interface between cardiac tissue and electrodes and McAdams et al. (1995) studied various different aspects of what happens when a metal is placed in an electrolyte. The most common circuit proposed for modeling the interface is shown in Fig. 5. The non faradic processes in the interface are represented by the double layer capacitance C_{dl} that corresponds to the layers of charge of opposite polarity located in the surface of the electrode and in the electrolyte. The faradic processes are represented by the charge transfer resistance R_{CT} in series with the Warburg impedance Z_W. The resistance R_{CT} represents the possible transfer of charge that occurs in the interface and Z_W represents the diffusion, with a transfer function as follows (where s stands for the Laplace variable):

$$Z_W = \frac{1}{C_w s^{0.5}} \tag{1}$$

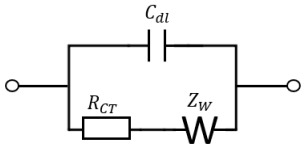

Fig. 5. Commonly used model for the electrode/electrolyte interface.

For the specific case of this study where platinum electrodes were chosen, the faradic processes are greatly reduced in the interface. Richardot and McAdams (2002) proposed a new circuit to represent specifically the case of platinum electrodes in electrolyte medium (Fig. 6).

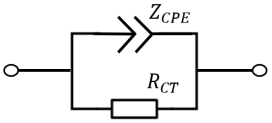

Fig. 6. Platinum electrode/electrolyte.

In this case, Z_{CPE} is a constant phase element of model (2) below, for $0 < \alpha < 1$ that represents the non faradic processes in the interface instead of the capacitance C_{dl}. The closest α is to 1 the closest the element is to a capacitor. The choice to replace the double layer capacitance by a constant phase element was made because the latter better represents the adsorption and surface roughness

effects. Even though the faradic processes are reduced, there might still be a charge transfer in very small amounts between the electrode and the electrolyte, as explained by Richardotand McAdams, that is why R_{CT} is still present in the circuit.

$$Z_{CPE} = \frac{1}{Qs^{\alpha}} \tag{2}$$

With the preliminary study of the EEG measurement chain made by Robinson and the interface proposed by Richardot and McAdams, the complete circuit that can represent the *phantom EEG* setup under study is given in Fig. 7. R_{m1}, Z_{CPE1}, and R_{CT1} represent the metallic resistance and the interface with the electrolyte for the input electrode, R_s represents the resistance of the solution (electrolyte), R_{m2}, Z_{CPE2}, and R_{CT2} represent the metallic resistance and the interface with the electrolyte for the output electrode, and C_s represents the shunt capacitance to the ground. Z_r is a simplification of the impedance of the recorder viewed from the measurement chain considering that the signal is filtered and amplified.

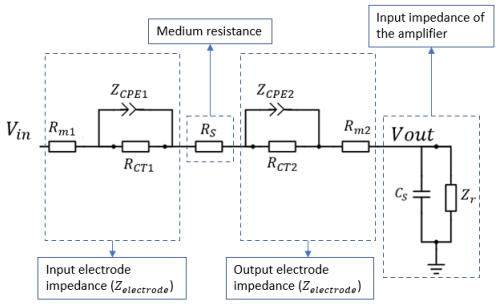

Fig. 7. Proposed model of the *phantom EEG* measurement chain.

For the case studied in this paper, the input and output electrodes will be considered to be the same in terms of their physical properties ($R_{m1} = R_{m2} = R_m$, $Z_{CPE1} = Z_{CPE2} = Z_{CPE}$, and $R_{CT1} = R_{CT2} = R_{CT}$). This consideration is made in order to simplify the model of the EEG measurement chain, as the identification of more complex models tend to be more sensitive to noise (as described in the results and discussion of this article.). This is not far from reality as both electrodes have the same dimensions, they are made of the same material and they are in contact with the same electrolyte. With this assumption, and using model (2) for Z_{CPE}, the impedance of each electrode can be represented as follows:

$$Z_{electrode} = \frac{R_m R_{CT} Q s^{\alpha} + R_m + R_{CT}}{R_{CT} Q s^{\alpha} + 1} = \frac{p_1 s^{\alpha} + p_2}{x_1 s^{\alpha} + 1} \tag{3}$$

3.2 Physical-based model considered for identification

The overall transfer function that describes the circuit given in Fig. 7, taking into consideration the impedance of the electrodes in equation (3) finally results in equation (4) below, with coefficients given in equation (5) to equation (9).

$$H(s) = \frac{V_{out}}{V_{in}} = \frac{b_1 s^{\alpha} + b_2}{a_1 s^{\alpha+1} + a_2 s + a_3 s^{\alpha} + 1} \tag{4}$$

$$b_1 = \frac{Z_r x_1}{Z_r + 2p_2 + R_s} \tag{5}$$

$$b_2 = \frac{Z_r}{Z_r + 2p_2 + R_s} \tag{6}$$

$$a_1 = \frac{2p_1 Z_r C_s + R_s Z_r C_s x_1}{Z_r + 2p_2 + R_s} \tag{7}$$

$$a_2 = \frac{2p_2 Z_r C_s + Z_r C_s R_s}{Z_r + 2p_2 + R_s} \tag{8}$$

$$a_3 = \frac{Z_r x_1 + 2p_1 + x_1 R_s}{Z_r + 2p_2 + R_s} \tag{9}$$

The aim now is to recover from the identification of transfer function (4), the six physical parameters of the circuit in Fig. 7 that are R_m, R_{CT}, Z_{CPE}, R_s, C_s, and Z_r. The problem is that there are only five coefficients which are (structurally) identifiable (see Walter and Pronzato (1997)) from equations (5) to (9). Therefore, one of the six physical parameters has to be estimated via other considerations. The chosen physical parameter to be calculated is the medium resistance R_s, which can be calculated directly from the general resistance formula given in equation (10) hereafter, in which σ ($[S/cm]$) is the electrical conductivity of the solution, l ($[cm]$) the length of the material for which the resistance is going to be measured and A ($[cm^2]$) the transverse surface of the material:

$$R = \frac{1}{\sigma}\frac{l}{A} \tag{10}$$

In the case of the resistance of the solution, the length (l) is the distance between the input and output electrodes. The area (A) is the transverse surface of electrolyte between the input and output electrodes, which can be approximated to the lateral surface of the cylinder of diameter 0.5 mm and height 0.5 cm. The electrical conductivity (σ) of the PBS presented in section 2 was already estimated in Johnson et al. (2005) as being $\sigma = 0.00181$ $[S/cm]$. The resulting values of the resistance of the solution in function of distance are given in table 1. The found values of R_s are close in order to those calculated in Robinson (1968) and Johnson et al. (2005).

Table 1. Values of R_s as a function of the distance between electrodes.

Distance between electrodes	R_s
1 cm	7.03 kΩ
3 cm	21.10 kΩ
5 cm	35.17 kΩ

With the resistance of the solution (R_s) known, the system of equations to recover the physical parameters of the circuit shown in Fig. 7 becomes:

$$\begin{cases} x_1 = \dfrac{b_1}{b_2} \\ Z_r(b_2 - 1) + 2p_2 b_2 = -R_s b_2 \\ 2p_1 - \dfrac{a_1}{b_2}\dfrac{1}{C_s} = -R_s \dfrac{b_1}{b_2} \\ \dfrac{a_2}{b_2}\dfrac{1}{C_s} - 2p_2 = R_s \\ Z_r\left(\dfrac{b_1}{b_2} - a_3\right) + 2p_1 - 2p_2 a_3 = R_s\left(a_3 - \dfrac{b_1}{b_2}\right) \end{cases} \tag{11}$$

3.3 Parameter identification of the transfer function

The chosen algorithm for the parametric identification of this system is the recursive least squares (RLS) with adaptation gain presented in Landau et al. (2011). This algorithm is chosen because from several experiments with the data obtained from the *phantom EEG* setup, it appeared to be more easily implemented, as compared to other ones, and with a satisfactory response for all cases satisfying the validation condition. The RLS is used to solve equations of the form given in equation (12) below, where the goal is to find the vector θ containing the coefficients (weights) that describe the transfer function. Vectors θ and ϕ for a rational transfer function are given in equations (13) and (14). Where N is the order of the denominator of the transfer function and M is the order of the numerator. The $\hat{}$ symbol represents the estimation as opposed to the real value of θ or $y(t+1)$.

$$\hat{y}(t+1) = \hat{\theta}^T \phi(t) \tag{12}$$

$$\hat{\theta}^T = [a_1, a_2, ..., a_N, b_1, b_2, ...b_M] \tag{13}$$

$$\begin{aligned} \phi^T = [&-y(t), -y(t-1), ..., -y(t+1-N), \\ &u(t+1), u(t), ..., u(t+1-M)] \end{aligned} \tag{14}$$

The recursive least squares algorithm with adaptation gain consists of the system (15), with λ representing the forgetting factor, meaning the given importance for past values in the current time estimation. In this application it is chosen as $\lambda = 0.99$ as it resulted in identified coefficients less sensitive to noise.

$$\begin{cases} \hat{\theta}(t+1) = \hat{\theta}(t) + F(t)\phi(t)\epsilon(t+1) \\ F(t+1) = \dfrac{1}{\lambda}[F(t) - \dfrac{F(t)\phi(t)\phi^T(t)F(t)}{\lambda + \phi^T(t)F(t)\phi(t)}] \\ \epsilon(k+1) = \dfrac{y(k+1) - \hat{\theta}^T(t)\phi(t)}{1 + \phi^T(t)F(t)\phi(t)} \end{cases} \tag{15}$$

In order to determine if an identified model is validated, in other words not biased, a test must be performed depending on the chosen identification method. The recursive least squares method is based on the whitening of the prediction error. Therefore, in order to validate the identified model, a whiteness test must be performed. The whiteness test consists in the verification of the whiteness of the prediction error $\epsilon(t)$. This can be done with the analysis of the normalized auto-correlations comparing them to a threshold value, which is relaxed to a global approximation of 0.15 as proposed by Landau et al. (2011).

In the case of this paper specifically, the system to be identified has a non integer order. Therefore, there are fractional order derivatives that need to be approximated in order to guarantee the precision of the identification. There are many ways in which one can approximate the non integer order derivative to a discrete equation, most of them are presented in Li and Zeng (2012), Malti et al. (2006), and Oustaloup (1995). A study prior to this article was done on the different equations of the non integer derivative approximation. The selected one was proposed by Ivo Petràš in Petráš (2011) for its small computational time and good precision.

The approximation consists of an IIR digital integer filter as an approximation of the fractional derivative of order α ($\alpha \in \mathbf{R}$). The resulting discrete transfer function is obtained via the continued fraction expansion (CFE) described in Petráš (2011) of the Al-Alaoui discretization of the fractional derivative described in Al-Alaoui (1993). In this procedure a generating function ω is chosen as the digital approximation of s^α ($s^\alpha \approx \omega(z^{-1})$). In Petráš (2011) the generating function is chosen as in equation (16) below, in which T represents the sampling time, r is the fractional order and a is a ratio term chosen as $a = 1/7$ as the Al-Alaoui rule for the discretization of s^α.

$$(\omega(z^{-1}))^{\pm r} = \left(\frac{1+a}{T}\frac{1-z^{-1}}{1+az^{-1}}\right)^{\pm r} \tag{16}$$

Applying the continued fraction expansion (CFE) in the generating function (16) one obtains equation (17) which ultimately results in equation (18), where c_i and d_i are the transfer function's coefficients and m and n are the respective nominator and denominator orders which are usually chosen to be the same:

$$(\omega(z^{-1}))^{\pm r} \approx \left(\frac{1+a}{T}\right)^{\pm r} CFE\left\{\left(\frac{1-z^{-1}}{1+az^{-1}}\right)^{\pm r}\right\}_{m,n} \tag{17}$$

$$(\omega(z^{-1}))^{\pm r} \approx \left(\frac{1+a}{T}\right)^{\pm r} \frac{c_0 + c_1 z^{-1} + \cdots + c_m z^{-m}}{d_0 + d_1 z^{-1} + \cdots + d_n z^{-n}} \tag{18}$$

The algorithm for this approximation already exists as a Matlab function developed by Ivo Petráš (Petráš (1993)) and is the one used in this study. As an input, the function *dfod1* takes the order of the equivalent transfer function to be found (N) and the weighting factor between the Euler, Tustin and Al-Alaoui rules (a). For the present case, the order is chosen as 4 and the weighting factor according to the Al-Alaoui rule (1/7). This values were chosen via trial and error by comparison of the responses of the identified models.

For the new model proposed in this study, there is not only non integer powers of the Laplace variable or non integer derivatives, but also, rational derivatives. In order to incorporate them in the final equation they need to be discretized as well. The chosen form of discretization is the Tustin one, because it has shown better results when used for identification compared to other ones. For this discretization, the Laplace variable s can be approximated as shown in equation (19), in which T is the sampling period:

$$s \approx \frac{2}{T}\frac{1-z^{-1}}{1+z^{-1}} \tag{19}$$

4. ESTIMATION RESULTS WITH EXPERIMENTAL DATA

The results obtained for the black box identification of the transfer function (4) will be presented considering the data obtained from *phantom EEG* experiments for all of the three distances between input and output electrodes. The first step is the determination of the non integer order α. To do that, a system is identified for various different fixed non integer orders in the interval $0 < \alpha < 1$. The order finally chosen is the one corresponding to the best identified system. The main criterion here considered for the comparison between identified systems is the best fitted Nyquist plot (when comparing model to data).

This criterion is chosen for the fact that the Nyquist plots analysis is subject to the largest variations under order changes, in comparison to time responses and bode plots. An example of Nyquist plots for a small interval of α values is given in Fig. 8 considering the distance of 1cm between electrodes. The selected non integer order is $\alpha = 0.8$. The same test was repeated considering the other distances and $\alpha = 0.8$ was selected as the optimal order for all of the cases. After this selection, the system identification is made, and the identified coefficients can be found in table 2.

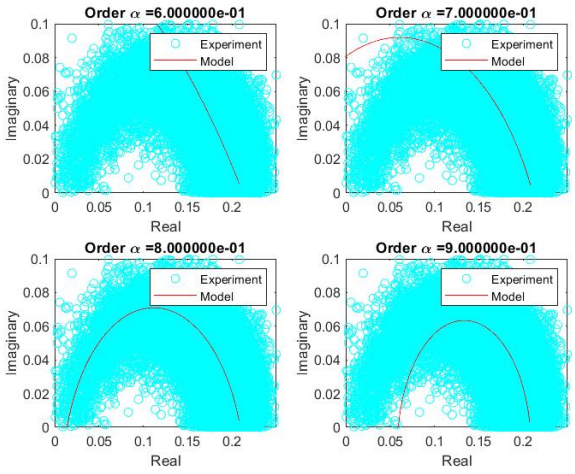

Fig. 8. Comparison between Nyquist plots for order selection (α).

Table 2. Identified coefficients with RLS method for each of the different distances.

	1cm	3cm	5cm
$\hat{b}_1$	1.0160e-03	5.3042e-04	3.7735e-04
$\hat{b}_2$	1.4043e-02	5.3900e-02	7.4789e-02
$\hat{a}_1$	-5.4077e-08	-8.1570e-08	-2.0437e-07
$\hat{a}_2$	7.3782e-09	9.1186e-09	1.1944e-08
$\hat{a}_3$	4.8536e-03	4.9977e-03	7.1832e-03

We identified $\hat{a}_1$ as negative for all of the distance cases, which we did not expected as the coefficients describe electronic components. However, since the value of $\hat{a}_1$ is really small when compared to $\hat{b}_1$, $\hat{b}_2$ and $\hat{a}_3$, it can be considered to be zero. With that, the system of equations given in (11) can be used to recover the physical parameters when R_s is considered known with values in table 1. However, the condition number of the matrix containing the weights of each variable is too high (1.9586e+09), which means that small variations in the results can imply big variations in the identified coefficients. In other words, the system is ill-conditioned and is not trustworthy to recover the physical parameters. This was also observed in simulation. As a remedy, a simplification of the model given by equation (4) can be considered. What can be seen from the obtained coefficients shown in table 2 indeed, is that not only $\hat{a}_1$ can be approximated as zero but also $\hat{a}_2$. With these remarks, only three coefficients will be next considered ($\hat{b}_1$, $\hat{b}_2$, and $\hat{a}_3$), and the transfer function can be rewritten as:

$$H(s) = \frac{b_1 s^\alpha + b_2}{a s^\alpha + 1} \tag{20}$$

Notice that the number of equations in the system is reduced, but C_s is no longer a variable to be identified, and, with R_s known there are only four physical parameters to be identified: R_m, R_{CT}, Z_{CPE} (that are combined to form p_1, p_2 and x_1), and Z_r. Even with a reduced number of parameters there is still one more physical parameter than equations, therefore R_m will be calculated. The calculation can indeed be done in the same way as that of R_s using equation (10). In this case σ is the electrical conductivity of platinum that can be found in Cantrell et al. (2008), l is the length of the electrode (1 cm) and A can be approximated as the transverse surface of the electrode assuming that the current flows uniformly inside it. With that, the value of the metallic resistance of the electrode is given by:

$$R_m = \frac{1}{9.4 \times 10^6} \frac{0.01}{\pi (2.5 \times 10^{-4})^2} = 0.0054 \ [\Omega] \tag{21}$$

The value of R_m is very small when compared to the other resistances, so it will not have an impact in the final physical values. The problem is that R_m is not written explicitly in the system of equations (11). But there is a way of expressing Z_r as a function of R_s and R_m. This can be achieved by dividing the coefficient b_1 of equation (5) by the coefficient a_3 of equation (9), and by writing p_1 and x_1 as functions of the electronic components. The system of equations (11) can be rewritten as (22):

$$\begin{cases} Z_r = \dfrac{(\frac{b_1}{a})2R_m + (\frac{b_1}{a})R_s}{1 - \frac{b_1}{a}} \\ x_1 = \dfrac{b_1}{b_2} \\ 2p_2 b_2 = -R_s b_2 - Z_r(b_2 - 1) \\ 2p_1 - 2p_2 a = R_s \left(a - \dfrac{b_1}{b_2}\right) - Z_r \left(\dfrac{b_1}{b_2} - a\right) \end{cases} \tag{22}$$

As the data for 3 cm and 5 cm of distance were found to have important noise, a new identification is done, considering only three parameters for these two cases, resulting in identified coefficients less sensitive to noise. The final coefficients identified for each of the cases are given in table 3. The coefficients were found not to be biased as they were validated by the whiteness test.

From these identified coefficients, equation (10), and the solution of (22), the physical parameters can be recovered

Table 3. Identified coefficients with RLS method for each of the different distances.

	1cm	3cm	5cm
$\hat{b}_1$	1.0160e-03	4.4200e-04	2.7536e-04
$\hat{b}_2$	1.4043e-02	1.2687e-02	5.7549e-03
$\hat{a}$	4.8536e-03	3.3536e-03	3.4787e-03

directly from the following system of equations, with l being the distance between input and output electrodes:

$$\begin{cases} R_s = (2.2099 \times 10^4)\, l \\ R_m = 0.0054 \\ Z_r = \dfrac{(\frac{b_1}{a})2R_m + (\frac{b_1}{a})R_s}{1 - \frac{b_1}{a}} \\ R_{CT} = p_2 - R_m \\ Q = \dfrac{x_1}{R_{CT}} \end{cases} \tag{23}$$

The solution of (23) gives the physical parameters summarized in table 4. The Nyquist plots for each case can be found in Fig.9.

Table 4. Physical parameters recovered from the results of the black box identification.

	1cm	3cm	5cm
R_s $[k\Omega]$	7.03	21.10	35.17
R_m $[\Omega]$	0.0054	0.0054	0.0054
R_{CT} $[k\Omega]$	61.86	114.10	243.58
Q $[Fs^{-1+\alpha}]$	1.17e-06	3.0534e-07	1.96e-07
Z_r $[k\Omega]$	1.86	3.20	3.02

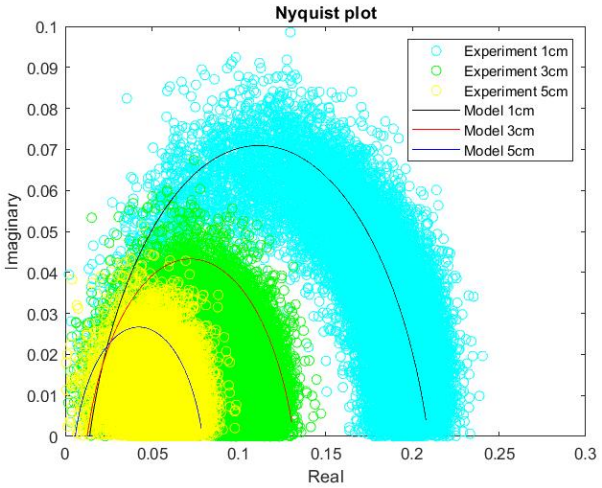

Fig. 9. Nyquist plots for all of the three distances between input and output electrodes.

5. CONCLUSIONS

In this paper a new dynamical model was proposed for the EEG measurement chain based on the physical properties of each separate part. The parametric identification together with the estimation of the medium and the electrodes resistances enabled the recovery of the values of the physical parameters, notably those of the electrode/electrolyte interface. Even though the model is more complex than the one proposed in previous studies, the separation into different parts allows its use in applications where the input signal comes from an unknown source, which is usually the case for EEG recordings.

Extensions to this work could be the use of the found model for better interpretation of the data obtained from EEG recordings in human patients, as the proposed model can be used for artefact correction. In applications of intracerebral stimulation, the interface electrode/tissue can still be represented by the same circuit as the electrode/electrolyte one according to Magin and Ovadia (2008). What can change in the overall circuit is the consideration of an additional layer called peri-electrode that is present for the cases of Deep Brain Stimulation (DBS) and the impedance of neural tissue.

REFERENCES

Al-Alaoui, M.A. (1993). Novel digital integrator and differentiator. *Electronics Letters*, 29(4), 376–378.

Becq, G., Voda, A., Besançon, G., Amblard, P.O., and Michel, O.J.J. (2017). Experiments and analysis for fractional order modelling of an EEG recording process. In *ICINCO*.

Besançon, G., Becq, G., and Voda, A. (2019). Fractional-order modeling and identification for a phantom EEG system. *IEEE Transactions on Control Systems Technology*, 1–9.

Besançon, G., Voda, A., Becq, G., and Machado, M.M.P. (2018). Order and parameter identification for a non-integer-order model of an EEG system. *IFAC-PapersOnLine*, 51. 18th IFAC Symposium on System Identification SYSID 2018.

Cantrell, D., Inayat, S., Taflove, A., Ruoff, R., and Troy, J. (2008). Incorporation of the electrode-electrolyte interface into finite-element models of metal microelectrodes. *Journal of neural engineering*, 5, 54–67.

Johnson, A., Sadoway, D., Cima, M., and Langera, R. (2005). Design and testing of an impedance-based sensor for monitoring drug delivery. *Journal of The Electrochemical Society - J ELECTROCHEM SOC*, 152.

Landau, I.D., Lozano, R., M'Saad, M., and Karimi, A. (2011). *Adaptive control: algorithms, analysis and applications-1rst édition*. Springer Science & Business Media.

Li, C. and Zeng, F. (2012). Finite difference methods for fractional differential equations. *International Journal of Bifurcation and Chaos*, 22.

Magin, R. and Ovadia, M. (2008). Modeling the cardiac tissue electrode interface using fractional calculus. *Journal of Vibration and Control*.

Malti, R., Aoun, M., Sabatier, J., and Oustaloup, A. (2006). Tutorial on system identification using fractional differentiation models. *IFAC Proceedings Volumes*, 39(1), 606 – 611. 14th IFAC Symposium on Identification and System Parameter Estimation.

McAdams, E., Lackermeier, A., McLaughlin, J., Macken, D., and Jossinet, J. (1995). The linear and non-linear electrical properties of the electrode-electrolyte interface. *Biosensors and Bioelectronics*.

Oustaloup, A. (1995). *La dérivation non entière - Théorie, synthèse et applications*. Hermes Science Publications.

Petráš, I. (2011). Fractional derivatives, fractional integrals, and fractional differential equations in Matlab. In A.H. Assi (ed.), *Engineering Education and Research Using MATLAB*, chapter 10. InTech.

Petráš, I. (1993). Digital fractional order differentiator/integrator – IIR type, Mathworks, inc. Matlab central file exchange.

Richardot, A. and McAdams, E. (2002). Harmonic analysis of low-frequency bioelectrode behavior. *IEEE transactions on medical imaging*.

Robinson, D.A. (1968). The electrical properties of metal microelectrodes. *Proceedings of the IEEE*, 56(6), 1065–1071.

Walter, E. and Pronzato, L. (1997). *Identification of parametric models from experimental data*. Springer, London.